Urban air quality: what is the optimal place to reduce transport emissions?

Tianyang Li[1], Sofia Fellini[2], Maarten van Reeuwijk[1,a]

[1] Department of Civil and Environmental Engineering, Imperial College London, SW7 2AZ London

[2] Univ Lyon, INSA Lyon, CNRS, Ecole Centrale de Lyon, Univ Claude Bernard Lyon 1, LMFA, UMR5509, 69621, Villeurbanne France.

[a] Email: m.vanreeuwijk@imperial.ac.uk

Abstract

We develop a linear model based on a complex network approach that predicts the effect of emission changes on air pollution exposure in urban street networks including NO-NO_2-O_3-chemisty. The operational air quality model SIRANE is used to create a weighted adjacency matrix A describing the relation between emissions of a passive scalar inside streets and the resulting concentrations in the street network. A case study in South Kensington (London) is used, and the adjacency matrix A_0 is determined for one wind speed and eight different wind directions. The physics of the underlying problem is used to infer A for different wind speeds. Good agreement between SIRANE predictions and the model is observed for all but the lowest wind speed, despite non-linearities in SIRANE's model formulation. An indicator for exposure in the street is developed, and it is shown that the out-degree of the exposure matrix E represents the effect of a change in emissions on the exposure reduction in all streets in the network. The approach is then extended to NO-NO_2-O_3-chemisty, which introduces a non-linearity. It is shown that a linearised model agrees well with the fully nonlinear SIRANE predictions. The model shows that roads with large height-to-width ratios are the first in which emissions should be reduced in order to maximise exposure reduction.

1. Introduction

Almost all the global population (99%) is exposed to pollution levels that exceed WHO limits, with middle- and low-income countries hit hardest (WHO, 2021). With the progressive shift of people from rural to urban areas, city administrations are urged to develop effective air quality plans to meet air quality standards and protect citizens' health. These plans mainly concern the control of vehicular traffic which is the most important source driving exceedances of air quality standards across city centres (EEA, 2022). For traffic control policies (Lu et al., 2021; Wu et al., 2017) to be effective, it is essential to quantify the contribution of local traffic emissions to the pollution levels of the urban area in order to optimally identify the places to impose restrictions. Methods for quantifying source-receptor relationship are known as source apportionment techniques (Wagstrom et al., 2008; Koo et al., 2009; Clappier et al., 2017) and the most common are based on simulations using air quality models.

Modelling air pollution in urban areas is far from trivial as flow and dispersion dynamics are strongly influenced by the presence of buildings, their geometric properties, and the orientation of the streets. Moreover, polluting emissions and exposure targets (i.e. citizens) are characterized by temporal and spatial patterns that make the analysis more complex. Further modelling issues are encountered when dealing with reactive pollutants. This is the case of nitrogen oxides (NO_2, NO) which are formed in combustion processes (mainly from vehicular traffic) and undergo a series of photochemical reactions with the secondary formation of ozone. Acute exposure to these pollutants causes respiratory diseases and paediatric asthma (Khreis et al., 2017; Anenberg et al., 2022). Since the reaction times of NO_2-NO-O_3 chemistry are comparable to their residence times in the streets (that is governed by turbulent transport) these transformations must be taken into account to predict air pollution at the district and street scales (Derwent & Middleton, 1996; Mchugh et al., 1997; Soulhac et al., 2011) and its impact on citizen's health.

Computational fluid dynamic (CFD) simulations can be effectively used to model flow, dispersion, and chemical reactions (Baker et al., 2004; Bright et al., 2013; Grylls et al., 2019; Zhang et al., 2020) in complex geometries. However, they are computationally expensive and require a large amount of detailed input data. The adoption of simplified modelling techniques is the most efficient option when dealing with urban areas consisting of hundreds of streets and when the goal is to explore multiple emission and exposure scenarios (Hertwig et al., 2018). The most widespread operational models are Gaussian models including parametrisations of urban effects (McHugh et al. 1997, Brook et al. 2003, Cimorelli et al. 2005), Lagrangian models able to represent the stochastic component of the dispersion process (Williams et al. 2004, Tinarelli et al. 2007), and the more recent street network models (Soulhac et al., 2011; Belcher et al. 2015; Kim et al., 2018). These are operational tools for air quality modelling based on the description of the urban fabric as a network of streets of homogeneous pollutant concentration. Each street is characterized by a polluting source and by the average geometric properties of the buildings. In this way, the complex urban pattern of buildings is represented by a simplified and regular domain of links (the streets) and nodes (street intersections). The wind flow and the turbulence in streets and street intersections are modelled by parametric relations on the network, while the concentration in the streets is estimated by a mass flow balance. Street network models have proven to be efficient for rapid prediction of air quality over large urban domains (Soulhac et al., 2012, Soulhac et al. 2017).

Fellini et al., 2019 developed a propagation model on networks to simulate pollutant dispersion from a point source using the same geometrical description as street network models. They used tools and metrics from complex network theory (Fellini et al., 2020, 2021) to unveil the physical mechanisms that drive dispersion processes and to detect vulnerable locations where a toxic gaseous release can

cause the greatest impact. In this paper, a similar methodology is used to predict the optimal location to reduce traffic emissions.

The theory of complex networks aims to describe a system as a network of interactions between its elements. These elements are represented by nodes, interconnected by links whenever a relationship is observed between the corresponding elements. The resulting network can then be described by means of multiple metrics or used as a basis for modelling. This theory has been successfully adopted in the field of urban science to investigate the topological properties of cities but also mobility patterns of citizens and socio-economic dynamics (Batty, 2013; Barthelemy, 2016). Recently, the complex network approach has proved useful in the study of geophysical flows, for example to analyse the motion of particles in turbulent flows (Iacobello et al., 2019; Ser-Giacomi et al., 2019).

Given the complexity of transport and transformation processes of pollutants in the urban atmosphere and the multiplicity of meteorological, emission and exposure scenarios, we propose in this work a network approach to model the relation between pollutant emissions and their impact on citizens and to perform source apportionment analyses. The aim is to answer the question: if a borough would like to reduce emissions in a neighborhood by a certain percentage, on which streets should action be taken in order to maximise the reduction in citizen's exposure? It will be demonstrated that due to the representation of emissions, air quality and exposure in the form of a complex network, multiple emissions and exposure scenarios can be easily simulated and the fundamental elements of the phenomenon are clearly identified.

The work is organized as follows: in section 2 the construction of the network is outlined together with the fundamental concepts of the model. Section 3 presents the case study to which the methodology is applied. Section 4 shows the potential of the model when dealing with a passive pollutant. In section 5, the method is extended to study exposure to reactive pollutants. Finally, in section 6, the conclusions and perspectives of the work are presented.

2. Methodology

2.1 Complex network representation

A weighted and directed network (Boccaletti et al., 2006) is adopted to model the correlation between pollutant emissions and concentration in the streets. In classical street network models, the network mimics the geometry of the urban fabric, with streets represented as links connecting two nodes that correspond to street intersections (Figure 1.a). Conversely, nodes represent here the streets while the directed links are the emission-impact relation between streets. Therefore, distant streets can also be connected (Figure 1.c) differently from the physical network of streets that is limited by the urban shape. The structure of the network is mathematically described by the adjacency matrix whose elements have a value equal to 1 or 0 depending on whether the pairs of nodes are connected or not in the graph. In addition to this information, the weight matrix A expresses for each non-zero value the weight (i.e. the importance) associated with the connection (Figure 1.d). The link weights therefore contain all the information relating to the transport of pollutants from one street to another.

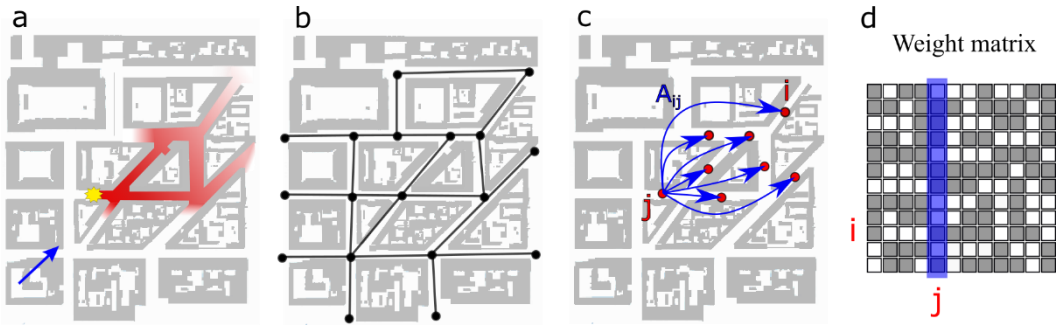


Figure 1: Schematic representation of pollutant dispersion in a dense city (a), the classical street-network domain (b), the emission-concentration network considered in this work (c) and the corresponding weight matrix (d). The non-zero elements in the blue column collect the concentration values in the contaminated streets from node j.

The main assumption underlying this work is that to first order, the transport within and between the streets can be represented as:

$$\boldsymbol{C} = A\boldsymbol{Q} \tag{1}$$

where $\boldsymbol{Q}$ and $\boldsymbol{C}$ are the transport emissions $[g/s]$ and concentration in each street $[\,\mu g/m^3\,]$ respectively, and A_{ij} is an entry of the weight matrix that represents how emissions in street j result in concentrations in street i. Denoting the number of streets by N, A is of size $N \times N$. Eq. (1) assumes that there is a linear relation between emissions and concentration, which is a hypothesis that will be tested later in the paper. Chemistry will create a nonlinear relation between $\boldsymbol{Q}$ and $\boldsymbol{C}$. This issue will be dealt with in Section 5. We note that Eq. (1) is equivalent to a source apportionment method as each row of A represents the linear weights of the sources contributing to the concentration in a street of the network.

2.2 Construction of the weight matrix A

The weight matrix A in Eq. (1) is constructed using the model SIRANE. SIRANE is an operational street network model for urban dispersion that has been adopted in several European cities and has been validated against both wind tunnel experiments and field campaigns (Carpentieri et al., 2012; Soulhac et al., 2003, 2012, 2017). The model is based on a simplified description of the urban geometry and adopts parametric relations to simulate the transport mechanisms of pollutants within the urban canopy. The streets of a city district are modelled as a network of boxes within which the pollutant is assumed to be uniformly mixed. Transport emissions in the street (Q) are taken into consideration as the source of pollution. The model simulates three main transport mechanisms: advection along the street axis (Q_{adv}), turbulent vertical exchange at the interface between the street and the overlying atmosphere ($Q_{H,turb}$), and exchange at street intersections (Q_I). The main physico-chemical processes are also modelled. These are the null-cycle chemistry and wet (Q_{wash}) and dry deposition (Q_{part}). The mass balance over each street volume for a passive scalar can be written as:

$$Q + Q_I = Q_{H,turb} + Q_{adv} + Q_{part} + Q_{wash}. \tag{2}$$

Above roofs, a Gaussian plume model is used. The interaction between the dispersion above roof and inside the street is mainly taken into account in the term $Q_{H,turb}$. SIRANE requires as input data the urban geometry, the meteorological conditions of the site, the background concentration of pollutants and the emissions within the streets. A meteorological pre-processor utilises parametrisations to simulate the boundary layer above roofs from the assigned conditions (Soulhac et al., 2011).

To construct the weight matrix A, we perform simulations with SIRANE on the urban district that will be presented in Section 0. We assume that the background concentration is zero and that the only

polluting source in the streets is the release of a gas behaving like a passive scalar. This is achieved using an ozone (O_3) emission in SIRANE, which, without the presence of any NO and NO_2, is an inert tracer in the model. We perform the simulations under neutral meteorological conditions, at a single wind speed U and one wind direction ϕ at a time. Under these assumptions, the *j*-th column of the weight matrix (Figure 1.c-d) is filled by simulating a unit ozone emission in the *j*-th street of the network. The resulting concentration values in the street network provides column j of matrix A. By repeating this operation for all the streets of the network, A is obtained. This procedure is then repeated for 8 wind directions, and A therefore depends on the intensity and direction of the wind above roofs, i.e. $A = A(U, \phi)$, as well as on the conditions of atmospheric stability. In practice, A is determined for one wind speed only, which we will refer to as the reference velocity U_0 and associated weight matrix $A_0(\phi) = A(U_0, \phi)$. The physics of the problem can be used to infer A at other wind speeds (see section 4.2).

2.3 Exposure

To find the best place to reduce emissions in the urban district, a metric is required that quantifies the exposure of citizens. Personal exposure depends sensitively on the type of pollutant, inhalation rate and duration of the exposure. Here, we adopt a simple measure for the exposure in a street e_i [g/hr] as:

$$e_i = p_i C_i q, \tag{3}$$

where p_i is the number of people living in street i (note that summation over repeated indices is not implied here) and q is the inhalation rate of a person, which is taken to be 0.571 m^3/hr (Epa & Factors Program, 2011). In matrix notation, this can be written as

$$\boldsymbol{e} = q\boldsymbol{p} \circ \boldsymbol{C} = q\boldsymbol{p} \circ A\boldsymbol{Q} = E\boldsymbol{Q}, \tag{4}$$

where $\circ$ is the Hadamard product[1] and $E_{ij} = qp_iA_{ij}$ is the exposure matrix. In this work, we will assume that the number of people p_i is constant as a function of time, but note that it is straightforward to consider different, more complex, scenarios (different days of the week, different hours) by changing the $\boldsymbol{p}$ vector only.

2.4 Street population estimation

To estimate the number of citizens in each street (p_i), we assume that the street is flanked by two buildings of constant width w, of length equal to the length of the street (L_i), and of height equal to the average depth of the street canyon H_i (panel c in Figure 2). We then assume a constant storey height H_F to assess the number of floors. The total living space for a street is thus given by:

$$S_i = 2\frac{H_i L_i w}{H_F}. \tag{5}$$

The corresponding resident population (p_i) can be calculated as the ratio between the living space and the average area per capita S_p, i.e. the average living space for a resident. This latter can be evaluated for a specific district as the ratio of the total living area given by the buildings in the district

[1] the Hadamard product is a binary operation that takes two matrices of the same dimensions and produces another matrix of the same dimension as the operands, where each element i, j is the product of elements i, j of the original two matrices, i.e. $A_{ij} = B_{ij}C_{ij}$ for every i, j.

$\sum_j 2\, H_j\, L_j w/H_F$ and the number of citizens n_{TOT} living in the district. Assuming a constant width for the buildings, we obtain the following expression for the number of people in street i:

$$p_i = 2\frac{H_i L_i w}{H_F}\frac{n_{TOT}}{2\, w \sum_j H_j L_j/H_F} = \frac{H_i L_i}{\sum_j H_j\, L_j} n_{TOT}. \quad (6)$$

In using the above street population estimation, we have implicitly assumed that the exposure of the people – who will spend most of their time indoors – is equal to as if they were outside of their homes. This assumption is correct if the outdoor concentration changes on timescales larger than the ventilation timescale. For residential buildings, the minimal recommended rate is 0.35 air changes per hour (ASHRAE, 2022), which implies the exposure assumption is valid for timescales larger than O(3) hours.

3. South Kensington case study

The case study (latitude 51.4998, longitude -0.1748) is located in South Kensington, a district west of central London, UK (Figure 2). The study area spans 672x1344 m^2 between Hyde Park and South Kensington station and is characterized by high population, developed transport and dense buildings. The high variety of morphological features (e.g., length of the streets, height of the buildings) and the different population density of the building blocks make this area suitable for investigating which places are most sensitive to the reduction of polluting emissions.

The representation of the urban district in SIRANE is detailed in Grylls et al., 2019. The street network is composed of 46 streets that are represented as straight links with starting and ending points located at the centre of the connecting intersections. Consistent with the description of the street as a box (see Section 2.2), each street has average geometric properties associated with it. The height (H) is given by the average height of the side buildings, while the street width (W) is the average distance between the lateral buildings (see Figure 2). Street length (L) is simply the distance between the two street intersections.

The geometrical properties of the street canyons are used to estimate the resident population according to Eq. (6). The total number of citizens n_{TOT} is estimated as the product of the district area and the average population density (12876 peo/km^2) of the reference region (Kensington and Chelsea) derived from Park (2020).

To construct matrix A for the study area, the simulations with SIRANE are performed for a neutrally stratified boundary layer. This is achieved in SIRANE by setting the albedo equal to 1. To simulate the dispersion of ozone as a passive scalar, we simulate night conditions: we set a temperature of 4 °C, a free stream wind velocity of 5 m/s and no precipitation. These conditions, together with null NO_X background concentrations, inhibit photochemical transformations (see Section 2.2). For the reactive scalar analysis, we consider daytime conditions: a winter day (January the 7th, T=14 °C) at noon, with partial cloud cover (5 Oktas). This condition was chosen for consistency with previous research (Grylls et al., 2019). Also in this case, we simulate a neutrally stratified atmosphere by setting the albedo equal to 1.

Vehicular emissions in the streets are estimated through the coupling of a VISSIM traffic microsimulation (Bloomberg & Dale, 2000) and the emission model developed by Int Panis et al. (2006). The resulting second-by-second NO_X emissions are time averaged over 1 hour and spatially averaged over the street boxes. Details are provided in Grylls et al. (2019). We adopted the total NO_X emissions as source term in the scalar dispersion analysis (Section 4). For the simulation of photochemical smog (Section 5), we applied an emission ratio $a = Q_{NO_2}/Q_{NO_x} = 0.2$ (Carslaw et al.,

2016; O'Driscoll et al., 2016; UK National Atmospheric Emission Inventory, 2018). In Figure 2(d), we report the values of NO_X emissions per street unit length adopted in this work. Moreover, for the reactive scalar analysis, realistic background concentrations were used. These were obtained as the average value in 2021 for the reference region (Kensington and Chelsea): $NO_2 = 34.26\ \mu g/m^3$, $NO = 17.09\ \mu g/m^3$ (UK Ambient Air Quality Interactive Map), $O_3 = 27.31 \mu g/m^3$ (Greater London Authority).

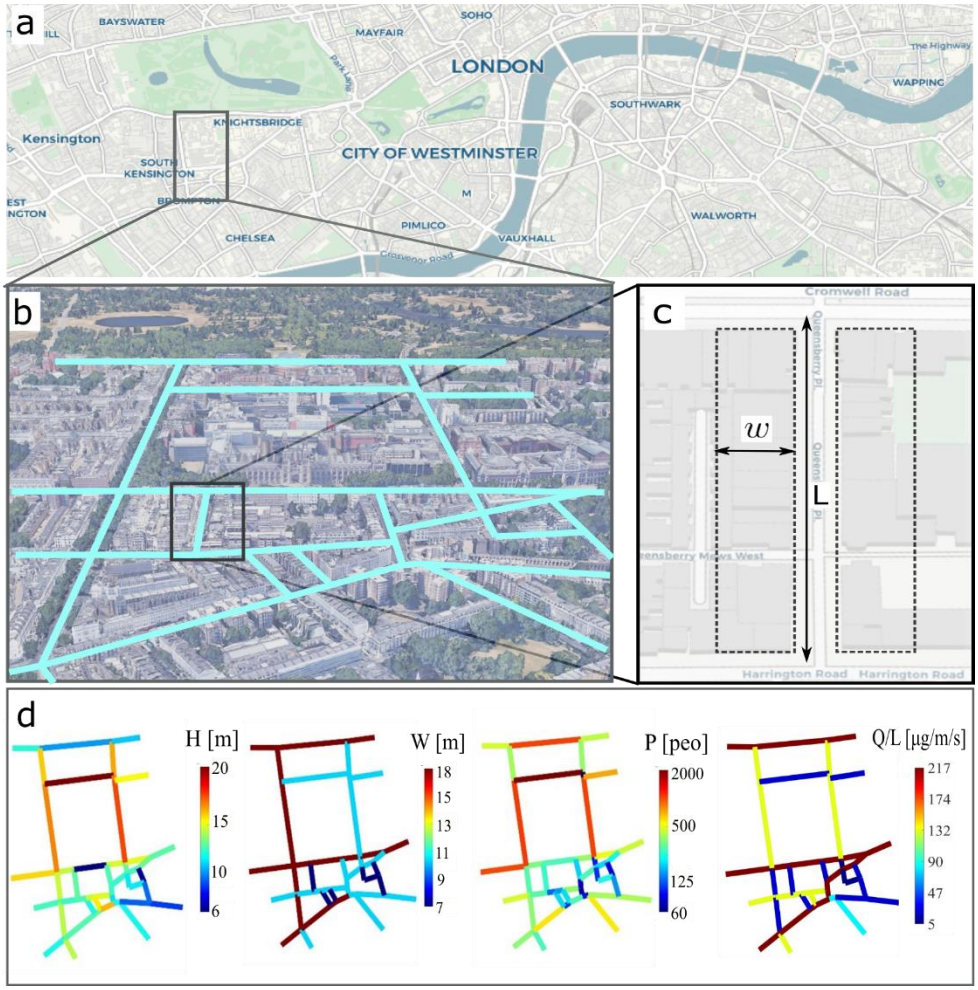


Figure 2: a) Location of South Kensington district in Central London. b) The study area and its street network. c) Schematization of lateral buildings for the estimation of the population. d) Depth (H) and width (W) of the street canyons. estimated population in the streets (P), and vehicular emissions per unit length of the street (Q/L).

4. Passive scalar transport

4.1 Concentration reconstruction

Following the method explained in Section 2.2, we construct the weight matrix A for the South Kensington district for eight different wind directions, assuming a constant wind speed $U_0 = 5$ m/s and neutral atmospheric stability conditions. In order to verify whether the resulting matrix is correct, we then perform a simulation in SIRANE with random emissions in multiple streets simultaneously (i.e. a random $\boldsymbol{Q}$ vector) and we compare the results with the concentration in the streets estimated using the linear model presented in Eq. (1). This comparative test is repeated 20 times and the results are reported in Figure 3(a), where each point represents the concentration in a single street for a specific wind direction and for an initial random distribution of emissions. The results show an excellent match between the two models which demonstrates that the system indeed is primarily linear and that the matrix approach has been implemented correctly.

The linearity of the system can be demonstrated by assuming a passive pollutant emitted on a rainless day (i.e. neglecting chemical reactions and dry and wet deposition) and with negligible re-entrainment of pollutants dispersed above roof levels, in which case the balance in Eq. (2) can be rewritten as:

$$Q + Q_I = Q_{H,turb} + Q_{adv} \rightarrow Q + U_S WHC_{up} = u_d WLC + U_S WHC, \tag{7}$$

where U_S and u_d are the advective velocity along the street canyon and the rate of vertical turbulent transfer at roof level, C and C_{up} are the average concentration in the street and in the airflow entering the street from the upwind intersection. The latter is in turn given by a linear superposition of the emissions in the upwind streets. These considerations evidence that the balance in Eq. (7) can be formulated as Eq. (1) and validate the very good correlation in Figure 3(a).

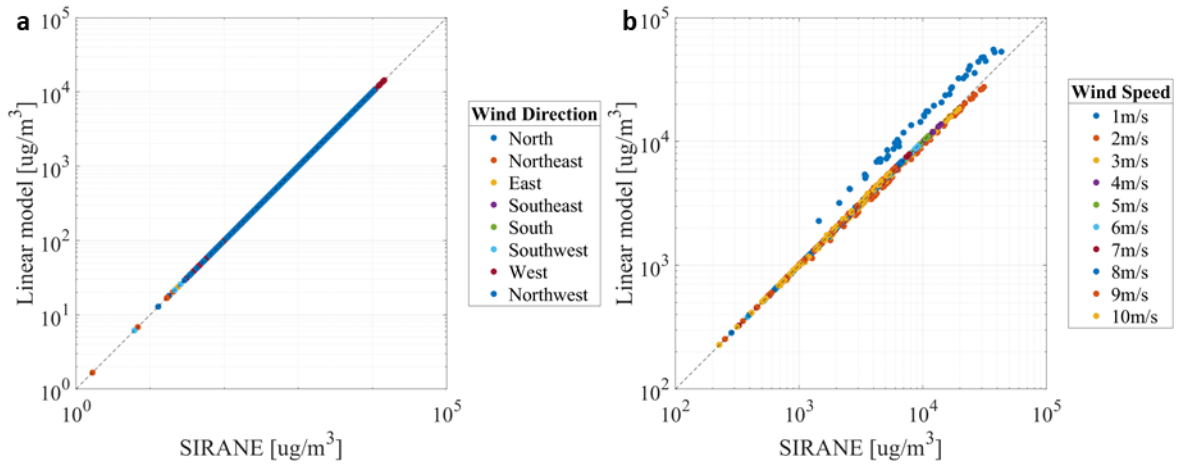


Figure 3: a) Concentration in the streets predicted by SIRANE and by the linear model proposed in Eq. (1) for different wind direction and a constant wind intensity (5 m/s). b) Simulation of different wind intensity scenarios by means of Eq. (8) and comparison with SIRANE. .

4.2 Wind speed correction

As highlighted by Eq. (7), the wind intensity affects the pollutant balance in the street by means of the two characteristic velocities U_S and u_d. Both these velocities can be parameterized, as a first approximation, as linear functions of the friction velocity (u_*) of the overlying boundary layer (Salizzoni et al., 2009 and Soulhac et al., 2010). Furthermore, assuming that the weather and stability of the atmosphere remain identical, the ratio between u_* and the free stream velocity (U) of the boundary layer is constant . These considerations suggest that matrix A in Eq. (1) is inversely proportional to the wind intensity U. Therefore, we can generalise the weight matrix A for a general wind speed as:

$$A(U, \phi) = \frac{U_0}{U} A_0(\phi) \tag{8}$$

where U_0 is the reference velocity (5 m/s in this study) and A_0 is the corresponding weight matrix. This scaling is adopted to simulate scenarios with ten different wind intensities, by using Eqs. (1) and (8). As for the reference case, random emissions $\boldsymbol{Q}$ are prescribed in the streets. The concentration predictions of Eq. (8) are compared in Figure 3(b) with the outcomes of the simulations performed with SIRANE. For each wind intensity, we take the average over the eight wind directions (ϕ). The agreement of (8) with SIRANE simulations at different wind speeds is excellent except for the case of a 1 m/s velocity. These differences are caused by the fact that SIRANE employs a minimum value for turbulent fluctuations (σ_v, σ_w) in the boundary layer. This is done to limit the errors of the street network model in case of low turbulence. This threshold applies in the 1 m/s scenario. For this reason, the vertical exchange velocity (which linearly depends on σ_w) is underestimated by the linear scaling

(Eq. (8)) compared to SIRANE prediction and leads to higher pollutant concentrations in the streets. Note that Eq. (8) is only valid under identical (neutral) boundary layer stability (see Section 0). Similar results can be expected for stable and convective conditions, although it should be carefully tested in future work.

4.3 Diagonal dominance of A

In this section we explore the diagonal dominance of matrix A, which is satisfied when $|A_{ii}|/\sum_{j\neq i}|A_{ij}| > 1$, i.e. the matrix is diagonally dominant when, for each row, the magnitude of the diagonal element in a row is larger than or equal to the sum of the magnitudes of all the other entries in that row. If A is found to be diagonally dominant, the concentration in the streets is mainly affected by local emissions. It should be noted that $|A_{ii}|/\sum_{j\neq i}|A_{ij}|$ tends to infinity as the matrix becomes diagonal. Therefore, to obtain a useful measure for the matrix as a whole, the harmonic mean of $|A_{ii}|/\sum_{j\neq i}|A_{ij}|$ for all the rows is taken:

$$D = \left(\frac{1}{N}\sum_{i}\frac{\sum_{j\neq i}|A_{ij}|}{|A_{ii}|}\right)^{-1}. \tag{9}$$

If $D > 1$ then the matrix is diagonally dominant on average. The harmonic mean weighs the smallest row values highest and will thus be a conservative estimate. By calculating D for all eight wind directions, we find that $133 < D < 193$, and thus conclude that self-interactions are expected to be very strong. Substitution of Eq. (8) shows that D is independent of wind velocity (provided the wind speed is not too small).

4.4 Reducing network complexity

The network contains a large number of links due to the transport of pollutants out of street canyons via the atmosphere and into street canyons downwind. The pollutant plume dilutes rapidly with downstream distance, resulting in a large number of very weak links. These can be removed without a noticeable impact on the concentration predictions. As demonstrated in the previous section, the matrix A is diagonally dominant, and we can use the mean of the diagonal entries to quantify the dominant interactions. We select a geometric mean $(\prod_1^N \mathrm{A}_{ii})^{\frac{1}{N}}$ to avoid one street dominating the mean as the diagonal entries can vary greatly in magnitude depending on the street properties. Introducing a threshold value α, the modified weight matrix $\breve{\mathrm{A}}_{ij}$ is determined as:

$$\breve{\mathrm{A}}_{ij} = \begin{cases} \mathrm{A}_{ij}, & if\ \mathrm{A}_{ij} > \alpha\left(\prod_1^N \mathrm{A}_{ii}\right)^{\frac{1}{N}} \\ 0, & \text{otherwise} \end{cases} \tag{10}$$

Figure 4(a) (blue curve) shows the trend in the number of links of matrix $\breve{\mathrm{A}}_{ij}$ as a function of α: using a threshold value $\alpha = 0.01$ decreases the number of links by a factor 3.28. The strong reduction in the number of links can be noticed in Figure 4(b) where the network under study is represented for three different exclusive thresholds. To quantify the error made due to link removal, we consider the relative error in the predicted concentration:

$$\epsilon = \frac{\|\boldsymbol{C} - \breve{\boldsymbol{C}}\|_2}{\|\boldsymbol{C}\|_2} = \frac{\|(A - \breve{A})\boldsymbol{Q}\|_2}{\|A\boldsymbol{Q}\|_2} \approx \frac{\|A - \breve{A}\|_2}{\|A\|_2}$$

where $\|\cdot\|_2$ is the L_2-norm, and the last step involves a change from a vector norm to a matrix norm. The relative error is adopted in order to emphasize differences in all the streets, as concentration varies greatly in the street network. The red curve in Figure 4 shows that the relative error ϵ is about 0.01 at $\alpha = 0.01$, and 0.05 at $\alpha = 0.1$. This demonstrates that the number of links can be reduced severely without significantly altering the properties of A. For large networks, using a small threshold value α will imply substantial savings in memory and an increase in computational performance. However, since the network considered here is small, we will not make use of the simplification.

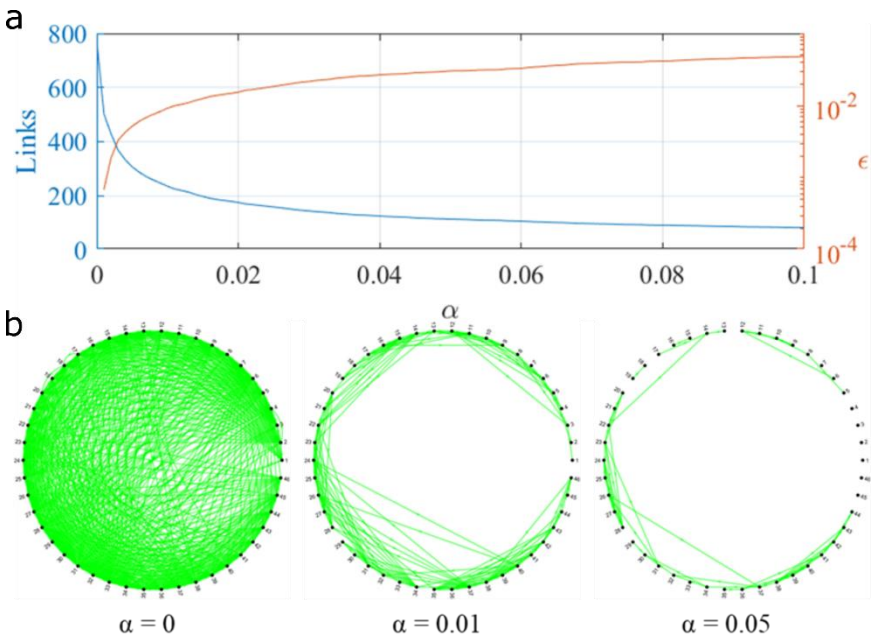


Figure 4: a) Number of links and error (ε) due to link removal for networks with different exclusive threshold α. b) Network representation for three different values of the exclusive threshold α.

4.5 Where to reduce emissions?

The scenario considered here is that a borough decides to reduce its total emissions by a certain amount and would like to know in which street this should be done in order to have the largest health benefits for its citizens. To answer this question, it is necessary to quantify the contribution of the emission in each street to the air pollution in the urban area. The process of evaluating the effect of a single source on the total concentrations is called source apportionment.

Following the source apportionment strategy, and in particular the tagged species approach (Wang et al., 2009; Grewe et al., 2010), we perturb the emission-exposure model introduced in Section 2 to analyse the exposure variation due to a change in the pollutant emissions as:

$$\delta \boldsymbol{e} = E \delta \boldsymbol{Q}. \tag{11}$$

The desired emission change is assumed to be $\delta Q = b\overline{Q}$ where $\overline{Q} = \frac{1}{N}\sum_i Q_i$ is the average emission rate per street and b is a parameter, which is taken to be 0.10 here. We are looking for the street j whose emission reduction $-\delta Q$ maximizes the sum of the exposure changes in all the streets. The total exposure reduction R_j due to an emission reduction $\delta Q_j = -\delta Q$ in street j can be expressed by:

$$R_j = -\sum_i \delta e_i = -\sum_k \delta Q_k \sum_i E_{ik} = \delta Q \sum_i E_{ij} \tag{12}$$

where the last step uses that δQ_k is different from 0 only in street j. Note that $\sum_i E_{ij}$ is formally defined in graph theory as the *outdegree* of node j (d_j^+), i.e. the sum of weights assigned to the links directed away from the node (Newman, 2010). So, the optimal place to reduce emissions corresponds to the node with the highest outdegree in the defined weighted network.

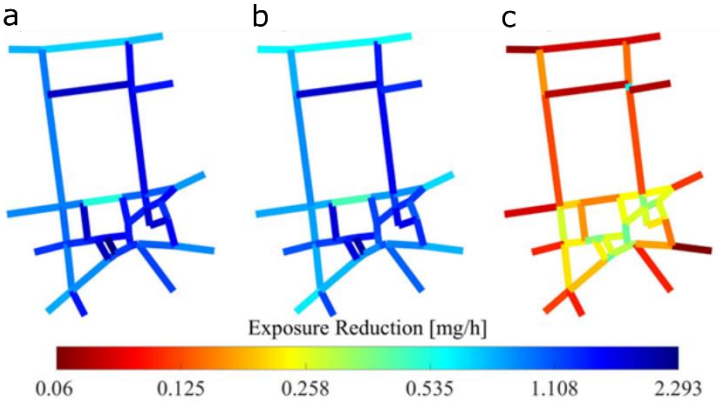


Figure 5: Exposure reduction achieved by decreasing the emission in the street by a constant quantity δQ. Panels a and b show the maximum and average values for the different wind directions. Panel c shows the average computed by neglecting self-interactions.

The exposure reduction ($\boldsymbol{R}$) is shown in Figure 5. In the analysis, we consider a single wind intensity $U_0 = 5$ m/s since we are interested in the variability of $\boldsymbol{R}$ among the streets and not in its absolute value. In this sense, the results shown in Figure 5 are also valid for the other wind intensities, in accordance with the linear relation in Eq. (8). To estimate δQ, we use the realistic emissions of NO_x in the streets (see Section 3). The reduction δQ is constant in all streets while the relative street emission reduction ($\delta Q/Q_i$) varies between 0.1 and 49%. Panels a and b show the maximum and average $\boldsymbol{R}$ for the different wind direction scenarios. The similarity between the two figures suggests that the results depend only weakly on the wind direction. This is likely because the main exposure reduction occurs in the same street where the emission is limited since matrix A (and thus E) is strongly diagonally dominant, as was shown in Section 4.3. To clarify this point, we report in panel c the results obtained by neglecting self-interactions in matrix *E*, i.e. for each street we compute the exposure reduction that is achieved in the whole network except in the street where the emission is reduced. The value of $\boldsymbol{R}$ is considerably lower in this case, confirming the importance of self-interactions.

The variability in the exposure reduction among the streets can be related to the geometry of the street canyons and their connectivity through an analytical argument. Since matrix A is strongly diagonally dominant, we can obtain an analytical expression for Eq. (12) considering self-interactions only, i.e. by neglecting pollutant exchange at street intersections:

$$R_i \approx \delta Q E_{ii} = \delta Q\, q\, p_i \frac{U_0}{U} A_{0,ii} = \frac{U_0}{U} \frac{\delta Q\, q\, p_i}{u_{d0} W_i L_i} = \frac{U_0}{U} \frac{\delta Q\, q\, n_{TOT}}{u_{d0} \sum_j H_j L_j} \frac{H_i}{W_i}. \quad (13)$$

The exposure reduction will be higher the higher the E_{ii} entry. This increases with the resident population in the street (p_i) and with the entry A_{ii} which provides the increase in pollutant concentration per unit emission. According to Eq. (6), p_i is a linear function of the length of the street and the height of the buildings. Following the model reported in Eq. (7) and considering again that there is no pollutant exchange at street intersections, we find that A_{ii} (here reported for a general wind intensity, i.e. $A = A_0 U_0/U$) decreases with W and L. Consequently, as demonstrated in Eq. (13), the exposure reduction is expected to scale with the street aspect ratio H/W, while the contribution of the street length should be negligible. This is confirmed by Figure 6, which shows a linear trend of

the exposure reduction with the canyon aspect ratio for the different scenarios of wind intensity (U). The dashed lines correspond to the prediction in Eq. (13). Panels *a* and *b* of Figure 5 evidence that R_j is not dependent on the street length.

When self-interactions are neglected (panel c), the exposure reduction in Eq. (12) is high when E_{ij} is different from zero for many *i,* i.e., when the interconnectivity of the network is high. For this reason, the largest exposure reductions in panel *c* are obtained on the well interconnected streets of the network.

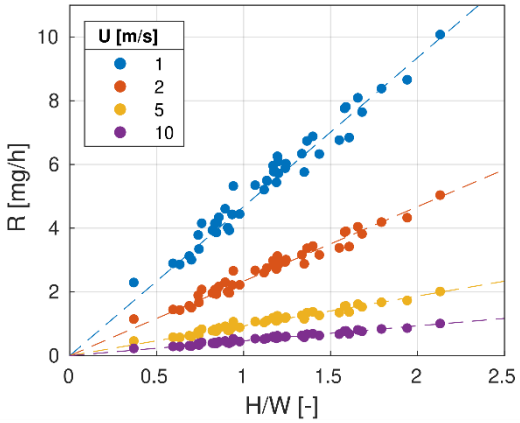


Figure 6: Exposure reduction (average over the wind directions) as a function of the aspect ratio (H/W) of the streets. Dashed lines correspond to the prediction in Eq. (13),

5. Extension to photochemical smog

The formalism will now be extended to include chemically reacting species, namely the $\mathrm{NO} - \mathrm{NO}_2 - \mathrm{O}_3$ cycle associated with photochemical smog (Oke et al., 2017). We follow SIRANE by assuming that the characteristic time scales of the chemical reactions are small compared to the residence time of pollutants within the streets. Under this assumption, a two-step method can be used to model the fate of the chemical species. First, we consider that ozone, nitric oxide and nitrogen dioxide are transported passively across the street network. After reaching the designated street, we assume that the species are in a photochemical steady state inside the canyon, and we apply chemical reactions to obtain the final concentration.

Adopting the network approach, the first step is the passive redistribution of chemical species, given by

$$\widetilde{\boldsymbol{C}}_{NO_2} = A\boldsymbol{Q}_{NO_2}, \quad \widetilde{\boldsymbol{C}}_{NO} = A\boldsymbol{Q}_{NO}, \quad \widetilde{\boldsymbol{C}}_{O_3} = A\boldsymbol{Q}_{O_3}, \tag{14}$$

where $\boldsymbol{Q}_X$ is the emission vector for species X in each street, $\widetilde{\boldsymbol{C}}_X$ is the vector for the passively advected concentration of species X, and A is the transport matrix (see Eq. (1)). Written in a single matrix multiplication, Eq. (14) becomes

$$\begin{bmatrix} \widetilde{\boldsymbol{C}}_{NO_2} \\ \widetilde{\boldsymbol{C}}_{NO} \\ \widetilde{\boldsymbol{C}}_{O_3} \end{bmatrix} = \begin{pmatrix} A & 0 & 0 \\ 0 & A & 0 \\ 0 & 0 & A \end{pmatrix} \begin{bmatrix} \boldsymbol{Q}_{NO_2} \\ \boldsymbol{Q}_{NO} \\ \boldsymbol{Q}_{O_3} \end{bmatrix}, \qquad \text{or simply} \quad \widetilde{\boldsymbol{C}} = B\boldsymbol{Q}. \tag{15}$$

The second step is to apply the chemistry which can be represented by

$$\boldsymbol{C} = \boldsymbol{f}(\widetilde{\boldsymbol{C}}), \tag{16}$$

where $\boldsymbol{f}$ is a nonlinear function that maps $\widetilde{\boldsymbol{C}}$ to $\boldsymbol{C}$ in each street. The null-cycle chemistry (Oke et al., 2017) together with the conservation of N and O species in a single street results in the following equilibrium concentrations:

$$\begin{aligned} [\mathrm{O_3}] &= \frac{-(k_3(c_N - c_O) + k_1) + \sqrt{\Delta}}{2k_3}, \\ [\mathrm{NO_2}] &= c_O - [\mathrm{O_3}], \\ [\mathrm{NO}] &= c_N - [\mathrm{NO_2}] = c_N - c_O + [\mathrm{O_3}], \end{aligned} \tag{17}$$

where

$$\begin{aligned} c_N &= \left[\widetilde{\mathrm{NO}}\right] + \left[\widetilde{\mathrm{NO_2}}\right] + [\mathrm{NO}]_b + [\mathrm{NO_2}]_b, \\ c_O &= \left[\widetilde{\mathrm{NO_2}}\right] + \left[\widetilde{\mathrm{O_3}}\right] + [\mathrm{NO_2}]_b + [\mathrm{O_3}]_b, \\ \Delta &= (k_3(c_N - c_O) + k_1)^2 + 4k_1k_3c_O. \end{aligned} \tag{18}$$

Here, the brackets denote molar concentrations, that are linked to the mass concentrations as $\tilde{X} = M_X[X]$, where M_X is the molar mass (g/mol) of species X. Here, $[X]_b$ is the background concentration of species X which is superimposed onto the passively advected concentration $[\tilde{X}]$ to provide the total molar concentration of N and O species, referred to as c_N and c_O. Furthermore, k_1 is the rate (expressed in $\mathrm{m^3mol^{-1}s^{-1}}$) of $\mathrm{NO_2}$ regeneration from NO and $\mathrm{O_3}$ reaction, and k_3 is the photolysis rate of $\mathrm{NO_2}$ (expressed in $\mathrm{s^{-1}}$). The two rates can be estimated as a function of the atmospheric temperature, cloud cover and solar elevation (e.g., Soulhac et al., 2011). Denoting $\tilde{\boldsymbol{c}}=\left[\widetilde{\mathrm{NO}}, \widetilde{\mathrm{NO_2}}, \widetilde{\mathrm{O_3}}\right]^T$ and $\boldsymbol{c}=[\mathrm{NO}, \mathrm{NO_2}, \mathrm{O_3}]^T$ as the mass concentration vectors in a single street before and after the chemical reaction, respectively, the relation between the two can be expressed as

$$\boldsymbol{c} = \boldsymbol{f_s}(\tilde{\boldsymbol{c}}) = \boldsymbol{f_s}\left(\widetilde{NO}, \widetilde{NO_2}, \widetilde{O_3}\right), \tag{19}$$

where $\boldsymbol{f_s}$ represents $\boldsymbol{f}$ for a single street. For the sake of clarity, we note that vector $\boldsymbol{c}$ is defined for each street and has 3 entries, while $\boldsymbol{C}$ (see Eq. (15)-(16)) is a vector of size $3N$, where N is the number of streets in the network.

There are a few specifics of air quality simulations that simplify the calculation of the term $\boldsymbol{f_s}$. First, ozone is a secondary pollutant, which implies that it is formed from reactions with primary pollutants and thus $\boldsymbol{Q}_{\mathrm{O_3}} = \boldsymbol{0}$, which in turn implies that $\widetilde{O_3} = 0$ (see Eq. (14)). We note that the background concentration of ozone is taken into account by means of Eq. (18). Second, the emissions of NO and $\mathrm{NO_2}$ are typically prescribed in terms of an emission ratio $a = Q_{NO_2}/Q_{NO_x}$ where a is a constant and $Q_{\mathrm{NO_x}}$ is reported on a $\mathrm{NO_2}$ basis (i.e. it is assumed that all NO is converted to NO_2). This means that

$$\boldsymbol{Q}_{\mathrm{NO}} = (1-a)\frac{M_{\mathrm{NO}}}{M_{\mathrm{NO_2}}}\boldsymbol{Q}_{\mathrm{NO_x}}, \qquad \boldsymbol{Q}_{\mathrm{NO_2}} = a\boldsymbol{Q}_{\mathrm{NO_x}}, \tag{20}$$

and, because of the linearity of A, that $\widetilde{\mathrm{NO}} = (1-a)\frac{M_{\mathrm{NO}}}{M_{\mathrm{NO_2}}}\widetilde{\mathrm{NO_x}}$ and $\widetilde{\mathrm{NO_2}} = a\widetilde{\mathrm{NO_x}}$. Thus, we can write

$$\boldsymbol{c} = \boldsymbol{f_s}\left(\widetilde{\mathrm{NO}}, \widetilde{\mathrm{NO_2}}, \widetilde{\mathrm{O_3}}\right) = \boldsymbol{g}\left(\widetilde{\mathrm{NO_x}}\right), \tag{21}$$

where $\boldsymbol{g}$ is a function that depends on the $\widetilde{\mathrm{NO_x}}$ concentration only.

To verify the two-step network model introduced above, we compare it with SIRANE. We note that also the chemical model currently implemented in SIRANE derives from the same assumptions (photostationary equilibrium in the canyon and NO and O balance). However, differently from SIRANE, we neglect the deposition of chemical species and all the dynamics of dispersion and transformation above roof levels. These assumptions are made to maintain a clear mathematical formulation, in line with the network description. In our model, the fate of the three species is predicted simply by using Eq. (15), i.e. matrix A from the passive scalar model, and by applying the function $\boldsymbol{g}$ for the chemical transformations.

As for the passive case, neutral atmospheric stability is enforced, which implies we can once more rely on matrix $A(U, \phi)$ for the transport. The chemical transformations are applied for a daytime scenario, i.e. the transformation rates k_1 and k_3 are estimated for January the 7th at noon, with partial cloud cover (5 Oktas) and a temperature of 14 °C. In SIRANE, we perform simulations for the reactive pollutants with the same meteorological conditions and by setting the surface albedo equal to 1 in order to recreate a neutrally stratified atmosphere even at noon.

To validate the photochemical model, we assign random emissions of $\mathrm{NO_x}$ in multiple streets and compare with the concentrations predicted by SIRANE. The emissions ratio $a = 0.2$ was assigned to the emissions in both models. Even in the case of chemical species, the concentrations are predicted with great accuracy for different wind directions (*Figure 7*(a)). Although it is not visible from *Figure 7*(a), the two-step network model gives a slightly higher prediction than SIRANE, about 2% in this data set. These slight deviations are because SIRANE takes into account the deposition of nitrogen oxides while the matrix A is constructed for a non-depositing passive scalar (see Section 2.2). In *Figure 7*(b), the linear scaling (Eq. (8)) for the wind intensity is used to simulate different velocity scenarios starting from a single matrix reconstruction (A_0 for $U_0 = 5$ m/s). The good agreement with the results from SIRANE shows that multiple wind intensity scenarios can be simulated starting from a single matrix A_0 even in the presence of chemical transformations. As mentioned in Section 4.1, the linear scaling for the wind intensity is valid only under the same stability conditions of the atmosphere since matrix A depends on them.

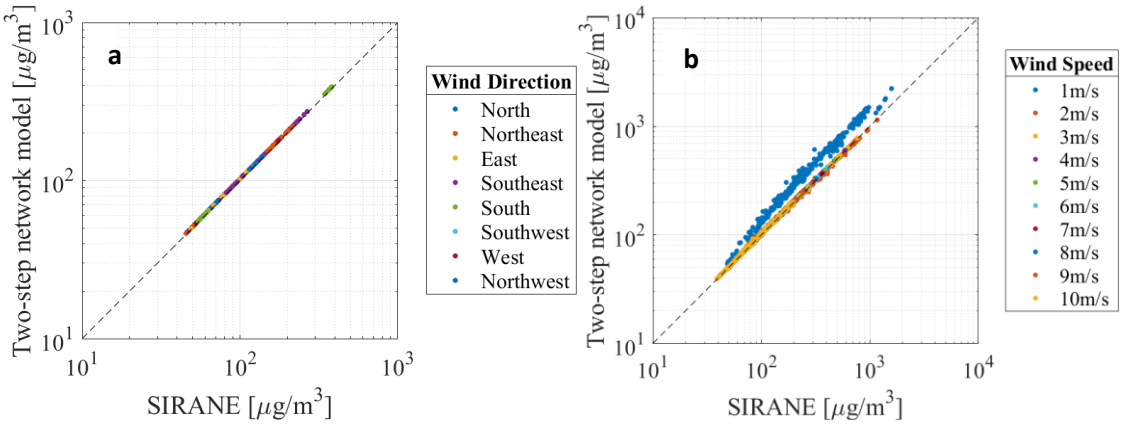


Figure 7: Concentration of NO2 in the streets predicted by SIRANE and by the two-step network model introduced in Eqs. (15)-(21). The comparison is made for simulations with different a) wind directions b) and wind speeds. For the results in panel (b), matrix A for the different wind intensities is simulated by means of Eq. (8).

5.1 Calculation of emission sensitivity

The inclusion of chemistry makes the exposure (Section 2.3) a nonlinear function of the emissions $\boldsymbol{Q}$:

$$\boldsymbol{e} = q\boldsymbol{p} \circ \boldsymbol{C} = q\boldsymbol{p} \circ \boldsymbol{f}(\widetilde{\boldsymbol{C}}) = q\boldsymbol{p} \circ \boldsymbol{f}(B\boldsymbol{Q}), \tag{22}$$

where we recall that q is the inhalation rate per person, $\boldsymbol{p}$ is the street population vector, $\boldsymbol{Q}$ is the street emissions vector, $\boldsymbol{f}$ is the function that applies the chemistry, and B is the matrix for passive advection of the three chemical species (see Eq. (16)). Exposure variation in the streets due to a change in the pollutant emissions can be expressed as

$$\delta \boldsymbol{e} = \boldsymbol{p} \circ \delta \boldsymbol{C} = \boldsymbol{p} \circ \delta \boldsymbol{f}(B\boldsymbol{Q}), \tag{23}$$

and a Taylor series expansion around the reference emissions $\boldsymbol{Q_0}$ results in

$$\delta \boldsymbol{e} = \boldsymbol{e} - \boldsymbol{e_0} \approx q\boldsymbol{p} \circ \frac{\partial \boldsymbol{f}}{\partial \widetilde{\boldsymbol{C}}} B\delta \boldsymbol{Q}, \tag{24}$$

or more succinctly

$$\delta \boldsymbol{e} = E\delta \boldsymbol{Q} \quad \text{where} \quad E = q\boldsymbol{p} \circ \frac{\partial \boldsymbol{f}}{\partial \widetilde{\boldsymbol{C}}} B. \tag{25}$$

Recalling that function $\boldsymbol{f}$ for a single street is denoted $\boldsymbol{f_s}$ for and that it can be simplified to $\boldsymbol{g}$ according to Eq. (21), the Jacobian is given by

$$\frac{\partial \boldsymbol{f_s}}{\partial \tilde{\boldsymbol{c}}} = \begin{pmatrix} \frac{\partial f_{s,1}}{\partial \tilde{c}_1} & \frac{\partial f_{s,1}}{\partial \tilde{c}_2} & \frac{\partial f_{s,1}}{\partial \tilde{c}_3} \\ \frac{\partial f_{s,2}}{\partial \tilde{c}_1} & \frac{\partial f_{s,2}}{\partial \tilde{c}_2} & \frac{\partial f_{s,2}}{\partial \tilde{c}_3} \\ \frac{\partial f_{s,3}}{\partial \tilde{c}_1} & \frac{\partial f_{s,3}}{\partial \tilde{c}_2} & \frac{\partial f_{s,3}}{\partial \tilde{c}_3} \end{pmatrix} = \frac{\mathrm{d}\boldsymbol{g}}{\mathrm{d}\widetilde{\mathrm{NO}}_\mathrm{x}} \begin{pmatrix} (1-a)\frac{M_{\mathrm{NO}}}{M_{\mathrm{NO_2}}} & a & 0 \end{pmatrix} \tag{26}$$

Figure 8 shows the sensitivity $\mathrm{d}\boldsymbol{g}/\mathrm{d}\widetilde{\mathrm{NO}}_\mathrm{x}$ for the photochemical equilibrium. Solid lines represent the model feedback when the background concentrations of the case study are considered. Dashed lines refer to the scenario with zero background concentrations. The starting position of the three component curves depends on the background concentration, while the asymptotic value for high $\widetilde{\mathrm{NO}}_\mathrm{x}$ concentration depends on the emission ratio *a*, i.e. when the emitted and advected nitrogen oxides ($\widetilde{\mathrm{NO}}_\mathrm{x}$) are very large, the background concentrations become negligible and the model behaves linearly (constant $\mathrm{d}\boldsymbol{g}/\mathrm{d}\widetilde{\mathrm{NO}}_\mathrm{x}$). We observe that $\mathrm{d}\boldsymbol{g}/\mathrm{d}\widetilde{\mathrm{NO}}_\mathrm{x}$ for ozone may be negative or positive. The negative(positive) $\mathrm{d}\boldsymbol{g}/\mathrm{d}\widetilde{\mathrm{NO}}_\mathrm{x}$ occurs when the background concentration of ozone ($[\mathrm{O}_3]_b$) is higher(lower) than the ozone concentration at equilibrium ($[\mathrm{O}_3]$). In any case, the rate of change of ozone always approaches zero as $\widetilde{\mathrm{NO}}_\mathrm{x}$ increases. This is due to the consumption of available ozone by nitrogen oxides and can be derived from equations (17)-(18) showing that $[O_3]$ goes to zero when $\widetilde{\mathrm{NO}}_\mathrm{x}$ tends to infinity. Finally, we remark that for the case study considered here, the ozone consumption decreases as the concentration of $\widetilde{\mathrm{NO}}_\mathrm{x}$ increases, which raises the risk associated with exposure to ozone (U.S. EPA, 2020).

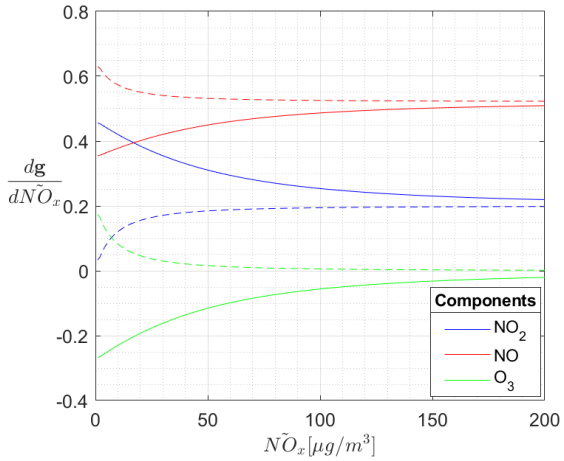


Figure 8 : Sensitivity of NO_2, NO *and* O_3 *concentration to the increase in the* $\widetilde{NO}_x$ *concentration according to Eq. (21). Zero background concentrations (dashed lines) and background concentrations of the case study* ($NO_2 = 34.26\ \mu g/m^3, NO = 17.09\ \mu g/m^3, O_3 = 27.31 \mu g/m^3$, *solid lines).*

5.2 Where to reduce emissions?

By substituting the emission sensitivity (26) into Eq. (25), it is straighforward to construct the emission matrix E for the scenario with photochemical smog and therefore the exposure reduction $\boldsymbol{R}$ by means of Eq. (12). Below, $\boldsymbol{R}$ is used to identify the best places to reduce emissions in the urban network. As in section 4.4, an emissions variation δQ = 0.10 $\bar{Q}$ is considered for both NO and NO_2 emissions, which are estimated from NO_X emissions (see Section 3) and by applying the emission ratio $a = 0.2$. Also in this case the relative emission reductions ($\delta Q/\boldsymbol{Q}$) vary between 0.1 and 49%.

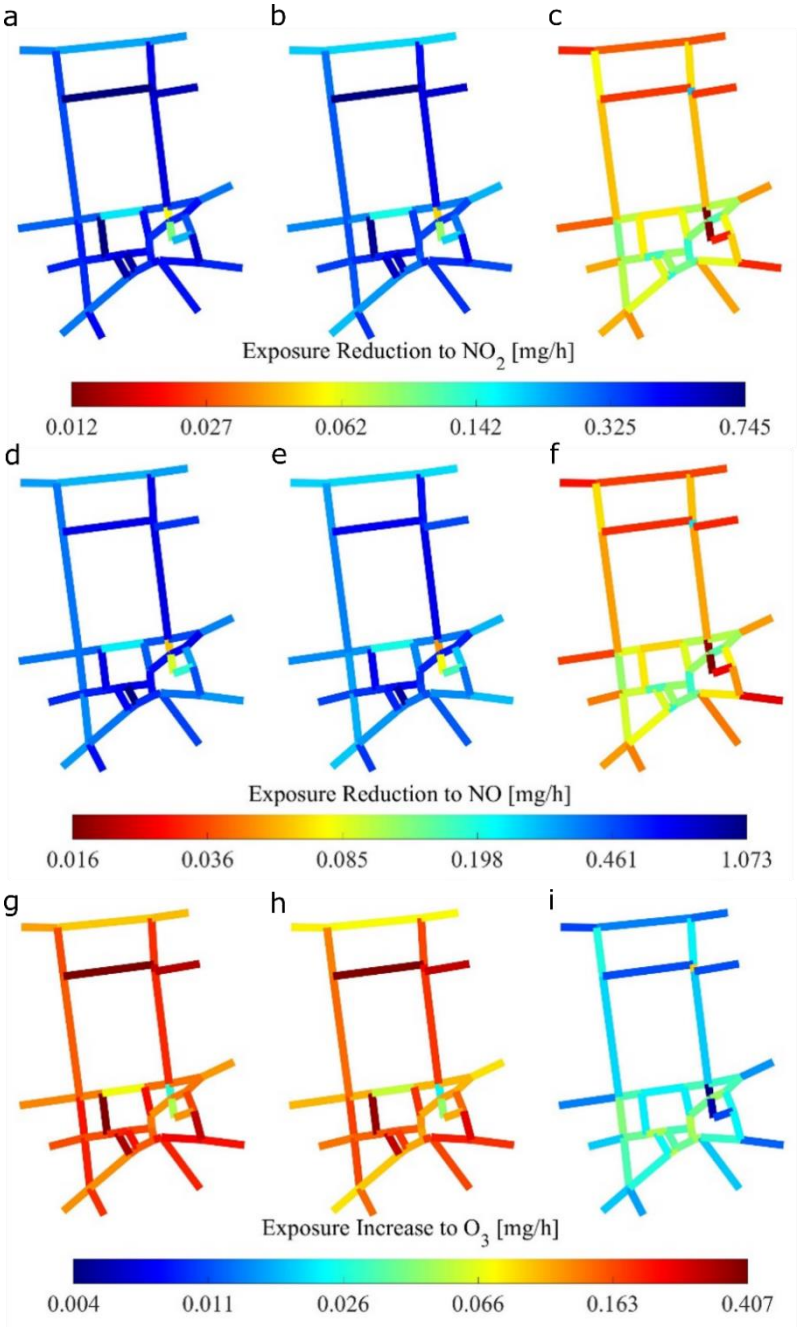


Figure 9: Exposure reduction achieved by decreasing the emission in the street by a constant quantity δQ for NO_2 (a-c) and NO (d-f). For O_3 the increase in exposure is shown in(g-i). (a,d,g) and (b,e,h) show the maximum and average values for the different wind directions. (c,f,i) show the average computed by neglecting self-interactions. Note the colorbar employs a logarithmic scaling.

Figure 9 shows the exposure reduction or increase for $\mathrm{NO_2}$, NO, and $\mathrm{O_3}$, in the South Kensington case study. As expected, a reduction δQ in $\mathrm{NO_x}$ emissions leads to an exposure reduction to nitrogen oxides (panels a-f). The results are very similar to the passive scalar case (Figure 5), and can nearly be reproduced using a single scaling factor per species. This is due to two reasons: (i) the relation between $\mathrm{NO_2}$ and $\widetilde{\mathrm{NO_2}}$ in the photostationary model is almost linear, especially for large $\widetilde{\mathrm{NO_2}}$ concentration (see Figure 8); and (ii) the background concentration and the ratio a are kept constant for all the streets. Consequently $d\boldsymbol{g}/\mathrm{d}\widetilde{\mathrm{NO}}_\mathrm{x}$ has almost constant entries and the matrix E in Eq. (25) is simply rescaled with respect to the case of the passive scalar.

On the other hand, panels g-i in Figure 9 evidence an exposure increase to ozone. This is in line with Figure 8 which shows a negative $d\boldsymbol{g}/\mathrm{d}\widetilde{\mathrm{NO}}_{\mathrm{x}}$ for ozone in the case study (solid lines). As explained above, this negative rate depends on the relation between the background and equilibrium ozone concentration. This result highlights that a side effect of the reduction of vehicular traffic may be an increase in ozone concentrations, depending on the background concentrations present in the area.

Finally, Figure 8 demonstrates that the sensitivity analysis presented in this section is dependent on the case study not only due to the dependence of $\mathrm{d}\boldsymbol{g}/\mathrm{d}\widetilde{\mathrm{NO}}_{\mathrm{x}}$ on the background concentration but also for its dependence on the initial emissions in the streets which provide the $\widetilde{\mathrm{NO}}_{\mathrm{x}}$ concentration (see Eqs. (14)-(15)) and may be characterized by different emission ratios *a.* When the emission ratio varies among the streets, $\mathrm{d}\boldsymbol{g}/\mathrm{d}\widetilde{\mathrm{NO}}_{\mathrm{x}}$ would no longer be a constant for the entire network (see Figure 8) and therefore the exposure reduction map in the case of chemical reactions (Figure 9) would be different from that obtained for the passive scalar (Figure 5). A similar conclusion would be reached if the emissions were low (small $\widetilde{\mathrm{NO}}_{\mathrm{x}}$ values) and the streets had different background concentrations. Again, according to Figure 8, the value of $\mathrm{d}\boldsymbol{g}/\mathrm{d}\widetilde{\mathrm{NO}}_{\mathrm{x}}$ would differ from street to street. These considerations pave the way for new simulations that investigate these aspects in order to draw non-site-specific conclusions.

Conclusions

In this work a complex network approach was used to address what is the optimal place to reduce emissions in an urban neighbourhood. Rather than developing a new air quality model, we introduced a mathematical formalism inspired by the theory of complex networks and based on the analysis of physical mechanisms, capable of extending the potential of existing operational tools. In fact, thanks to our approach, it is ultimately possible to reconstruct a large multiplicity of scenarios starting from a single dispersion simulation of a passive scalar.

The network was defined by modelling the correlation between emissions and concentrations in streets as weighted links connecting the streets, i.e. the nodes of the network. In this way, the entire process of pollutant dispersion was enclosed in the weight matrix A of the network. By means of this formulation the hypothesis of linearity between emissions and concentrations in the case of non-reactive pollutants was first tested. Then, considering the physics underlying the process, we proposed a linear scaling of matrix A with the intensity of the external wind. This relation is valid only under identical atmospheric stability conditions. Under this assumption, scenarios with different emissions in the streets and different intensity of the external wind could be reproduced using a single weight matrix A_0 constructed from a single dispersion simulation. The network model highlighted the diagonal-dominancy of the problem and suggested a criterion to significantly reduce the computational complexity of the solution, eliminating the less significant network connections.

The network description facilitated straightforward translation from pollution levels (concentrations) to citizen exposure: a new weight matrix, the exposure matrix, was derived starting from A which took into account the number of people exposed in each street. The outdegree of this new matrix provided a direct metric for exposure reduction in terms of which streets bring the greatest benefits in terms of health impact at the neighbourhood scale.

Finally, the model was extended to the analysis of photochemical smog. We used a two-step algorithm to reconstruct the concentrations of reactive pollutants in the streets by applying matrix *A* and a non-linear function for chemical transformations in the streets. Through a linearization of the exposure model, we obtained an expression of the exposure reduction metric for reacting chemical species and

showed that it can be approximated with a rescaling of the metric for the passive case. This scaling is valid only if the background concentration and the emission ratio are kept constant for each street.

The exposure model used in combination with the diagonal dominance of A gave clear indication of what generally the most effective strategy is in terms of health: to reduce emissions in domestic streets with the high aspect ratio H/W, e.g. by making the street one-way. This conclusion holds if we assume that the population in a street scales linearly with the height of the buildings and the length of the street. Indeed, under this assumption, the exposure estimate in Eq. (13) is an accurate measure that can be used to estimate total exposure in a street in an operational sense without even the need for a network model.

The simplicity of the proposed derivation and the modularity of the model make it suitable to be improved in its parts and to be applied to more realistic scenarios. Firstly, the emission scenario could account for emission reductions in multiple streets rather than a single street, or different background concentrations and/or emission ratios in the streets. Secondly, the study could be easily tested and extended to different atmospheric stability conditions and to different photochemical models as the conclusions of this work are valid only in the case of a neutral atmosphere in stationary photochemical conditions. Thirdly, the relationship between the level of pollution and the exposure of citizens in the street could be improved as it is currently based on two approximations: the assumption that indoor and outdoor exposure coincide and that the number of citizens in a street is a simple function of the canyon geometry. Finally, matrix A could be estimated with more accurate dispersion simulations (e.g., LES simulations). Although computationally more expensive than SIRANE, a single run would be sufficient to then simulate multiple scenarios by means of the proposed linear model.

In conclusion, the adoption of a network approach brings significant benefits: it provides a new perspective on a classical problem and it suggests new metrics that can bring new insights into the analysis of the results and guide administrations in traffic and emission management.

Acknowledgements

The authors would like to thank Prof. Lionel Soulhac for providing a custom version of SIRANE suitable for source apportionment and for insightful conversations about data assimilation. MvR would like to thank Prof. Pietro Salizzoni for the opportunity to visit their group in Lyon as a visiting Professor in 2022.

Bibliography

Anenberg, S. C., Mohegh, A., Goldberg, D. L., Kerr, G. H., Brauer, M., Burkart, K., Hystad, P., Larkin, A., Wozniak, S., & Lamsal, L. (2022). Long-term trends in urban NO2 concentrations and associated paediatric asthma incidence: estimates from global datasets. *The Lancet Planetary Health*, *6*(1), e49–e58. https://doi.org/10.1016/S2542-5196(21)00255-2.

ASHRAE. (2013). *ANSI/ASHRAE Standard 62.2-2022 Ventilation and acceptable indoor air quality in residential buildings*. Peachtree Corners, GA: American Society of Heating, Refrigerating and Air-Conditioning Engineers.

Baker, J., Walker, H. L., & Cai, X. (2004). A study of the dispersion and transport of reactive pollutants in and above street canyons—a large eddy simulation. *Atmospheric Environment*, *38*(39), 6883–6892.

Barthelemy, M. (2016). *The structure and dynamics of cities*. Cambridge University Press.

Batty, M. (2013). *The new science of cities*. MIT press.

Belcher, S. E., Coceal, O., Goulart, E. V., Rudd, A. C., & Robins, A. G. (2015). Processes controlling atmospheric dispersion through city centres. *Journal of Fluid Mechanics*, *763*, 51-81.

Bloomberg, L., & Dale, J. (2000). Comparison of VISSIM and CORSIM Traffic Simulation Models on a Congested Network. *Transportation Research Record: Journal of the Transportation Research Board*, *1727*(1), 52–60. https://doi.org/10.3141/1727-07

Boccaletti, S., Latora, V., Moreno, Y., Chavez, M., & Hwang, D.-U. (2006). Complex networks: Structure and dynamics. *Physics Reports*, *424*(4–5), 175–308.

Bright, V. B., Bloss, W. J., & Cai, X. (2013). Urban street canyons: Coupling dynamics, chemistry and within-canyon chemical processing of emissions. *Atmospheric Environment*, *68*, 127–142.

Brook, D., Felton, N., Clem, C., Strickland, D., Griffiths, I., Kingdon, R., Hall, D., & Hargrave, J. (2003). Validation of the urban dispersion model (UDM). *International Journal of Environment and Pollution* 20(1–6):11–21.

Carpentieri, M., Salizzoni, P., Robins, A., & Soulhac, L. (2012). Evaluation of a neighbourhood scale, street network dispersion model through comparison with wind tunnel data. *Environmental Modelling and Software*, *37*, 110–124. https://doi.org/10.1016/j.envsoft.2012.03.009

Cimorelli, A. J., Perry, S. G., Venkatram, A., Weil, J. C., Paine, R. J., Wilson, R. B., Lee, R. F., Peters, W. D., & Brode, R. W. (2005). AERMOD: A dispersion model for industrial source applications. Part I: General model formulation and boundary layer characterization. *Journal of applied meteorology*, 44(5), 682-693.

Clappier, A., Belis, C. A., Pernigotti, D., & Thunis, P. (2017). Source apportionment and sensitivity analysis: two methodologies with two different purposes. *Geoscientific Model Development*, *10*(11), 4245–4256. https://doi.org/10.5194/gmd-10-4245-2017

Derwent, R. G., & Middleton, D. R. (1996). An empirical function for the ratio NO sub (2): NO sub (x). *Clean Air*, *26*(3), 57–60.

EEA. (2022). *Managing air quality in Europe*.

Epa, U., & Factors Program, E. (2011). *Exposure Factors Handbook: 2011 Edition*. www.epa.gov

Fellini, S., Salizzoni, P., & Ridolfi, L. (2020). Centrality metric for the vulnerability of urban networks to toxic releases. *Physical Review E*, *101*(3), 32312.

Fellini, S., Salizzoni, P., & Ridolfi, L. (2021). Vulnerability of cities to toxic airborne releases is written in their topology. *Scientific Reports*, *11*(1). https://doi.org/10.1038/s41598-021-02403-y

Fellini, S., Salizzoni, P., Soulhac, L., & Ridolfi, L. (2019). Propagation of toxic substances in the urban atmosphere: A complex network perspective. *Atmospheric Environment*, *198*, 291–301.

Greater London Authority. (n.d.). *London Average Air Quality Levels - London Datastore*. Retrieved April 1, 2022, from https://data.london.gov.uk/dataset/london-average-air-quality-levels

Grewe, V., Tsati, E., & Hoor, P. (2010). On the attribution of contributions of atmospheric trace gases to emissions in atmospheric model applications. *Geoscientific Model Development*, *3*(2), 487–499. https://doi.org/10.5194/gmd-3-487-2010

Grylls, T., le Cornec, C. M. A., Salizzoni, P., Soulhac, L., Stettler, M. E. J., & van Reeuwijk, M. (2019). Evaluation of an operational air quality model using large-eddy simulation. *Atmospheric Environment: X*, *3*, 100041. https://doi.org/10.1016/J.AEAOA.2019.100041

Hertwig, D., Soulhac, L., Fuka, V., Auerswald, T., Carpentieri, M., Hayden, P., Robins, A., Xie, Z-T., & Coceal, O. (2018). Evaluation of fast atmospheric dispersion models in a regular street network. *Environmental Fluid Mechanics*, 18(4), 1007-1044.

Iacobello, G., Marro, M., Ridolfi, L., Salizzoni, P., & Scarsoglio, S. (2019). Experimental investigation of vertical turbulent transport of a passive scalar in a boundary layer: Statistics and visibility graph analysis. *Physical Review Fluids*, *4*(10), 104501.

Int Panis, L., Broekx, S., & Liu, R. (2006). Modelling instantaneous traffic emission and the influence of traffic speed limits. *Science of The Total Environment*, *371*(1–3), 270–285. https://doi.org/10.1016/j.scitotenv.2006.08.017

Khreis, H., Kelly, C., Tate, J., Parslow, R., Lucas, K., & Nieuwenhuijsen, M. (2017). Exposure to traffic-related air pollution and risk of development of childhood asthma: A systematic review and meta-analysis. In *Environment International* (Vol. 100, pp. 1–31). Elsevier Ltd. https://doi.org/10.1016/j.envint.2016.11.012

Kim, Y., Wu, Y., Seigneur, C., & Roustan, Y. (2018). Multi-scale modeling of urban air pollution: development and application of a Street-in-Grid model (v1. 0) by coupling MUNICH (v1. 0) and Polair3D (v1. 8.1). *Geoscientific Model Development*, *11*(2), 611–629.

Koo, B., Wilson, G. M., Morris, R. E., Dunker, A. M., & Yarwood, G. (2009). Comparison of Source Apportionment and Sensitivity Analysis in a Particulate Matter Air Quality Model. *Environmental Science & Technology*, *43*(17), 6669–6675. https://doi.org/10.1021/es9008129

Lu, J., Li, B., Li, H., & Al-Barakani, A. (2021). Expansion of city scale, traffic modes, traffic congestion, and air pollution. *Cities*, *108*, 102974. https://doi.org/10.1016/j.cities.2020.102974.

McHugh, C. A., Carruthers, D. J., & Edmunds, H. A. (1997). ADMS–Urban: an air quality management system for traffic, domestic and industrial pollution. *International Journal of Environment and Pollution*, *8*(3–6), 666–674.

Newman, M. (2010). *Networks*. Oxford University Press. https://doi.org/10.1093/acprof:oso/9780199206650.001.0001

Oke, T. R., Mills, G., Christen, A., & Voogt, J. A. (2017). *Urban Climates*. Cambridge University Press. https://doi.org/10.1017/9781139016476

Park, N. (2020). Population-estimates-for-the-UK-England-and-Wales-Scotland-and-Northern-Ireland-provisional-mid-2019. *Hampshire: Office for National Statistics*.

Salizzoni, P., Soulhac, L., & Mejean, P. (2009). Street canyon ventilation and atmospheric turbulence. *Atmospheric Environment*, *43*(32), 5056–5067. https://doi.org/10.1016/j.atmosenv.2009.06.045

Ser-Giacomi, E., Baudena, A., Rossi, V., Vasile, R., Lopez, C., & Hernández-Garca, E. (2019). From network theory to dynamical systems and back: Lagrangian Betweenness reveals bottlenecks in geophysical flows. *ArXiv Preprint ArXiv:1910.04722*.

Soulhac, L., Nguyen, C. v., Volta, P., & Salizzoni, P. (2017). The model SIRANE for atmospheric urban pollutant dispersion. PART III: Validation against NO2 yearly concentration measurements in a large urban agglomeration. *Atmospheric Environment*, *167*, 377–388. https://doi.org/10.1016/j.atmosenv.2017.08.034

Soulhac, L., Puel, C., Duclaux, O., & Perkins, R. J. (2003). Simulations of atmospheric pollution in Greater Lyon an example of the use of nested models. *Atmospheric Environment*, *37*(37), 5147–5156. https://doi.org/10.1016/j.atmosenv.2003.03.002

Soulhac, L., & Salizzoni, P. (2010). Dispersion in a street canyon for a wind direction parallel to the street axis. *Journal of Wind Engineering and Industrial Aerodynamics*, *98*(12), 903–910. https://doi.org/10.1016/j.jweia.2010.09.004

Soulhac, L., Salizzoni, P., Cierco, F. X., & Perkins, R. (2011). The model SIRANE for atmospheric urban pollutant dispersion; part I, presentation of the model. *Atmospheric Environment*, *45*(39), 7379–7395. https://doi.org/10.1016/j.atmosenv.2011.07.008

Soulhac, L., Salizzoni, P., Mejean, P., Didier, D., & Rios, I. (2012). The model SIRANE for atmospheric urban pollutant dispersion; PART II, validation of the model on a real case study. *Atmospheric Environment*, *49*, 320–337. https://doi.org/10.1016/j.atmosenv.2011.11.031

Tinarelli, G., Brusasca, G., Oldrini, O., Anfossi, D., Castelli, S. T., & Moussafir, J. (2007). Micro-Swift-Spray (MSS): a new modelling system for the simulation of dispersion at microscale. General description and validation. In *Air pollution modeling and its application XVII* (pp. 449-458). Springer, Boston, MA.

UK Ambient Air Quality Interactive Map. (n.d.). Retrieved April 1, 2022, from https://uk-air.defra.gov.uk/data/gis-mapping/

U.S. EPA. (2020). *Integrated Science Assessment (ISA) for Ozone and Related Photochemical Oxidants (Final Report, Apr 2020)*.

Wagstrom, K. M., Pandis, S. N., Yarwood, G., Wilson, G. M., & Morris, R. E. (2008). Development and application of a computationally efficient particulate matter apportionment algorithm in a three-dimensional chemical transport model. *Atmospheric Environment*, *42*(22), 5650–5659. https://doi.org/10.1016/J.ATMOSENV.2008.03.012

Wang, Z. S., Chien, C.-J., & Tonnesen, G. S. (2009). Development of a tagged species source apportionment algorithm to characterize three-dimensional transport and transformation of precursors and secondary pollutants. *Journal of Geophysical Research*, *114*(D21). https://doi.org/10.1029/2008jd010846

WHO. (2021). *WHO global air quality guidelines: particulate matter (PM2. 5 and PM10), ozone, nitrogen dioxide, sulfur dioxide and carbon monoxide*.

Williams, M. D., Brown, M. J., Singh, B., & Boswell, D. (2004). QUIC-PLUME theory guide. *Los Alamos National Laboratory*, 43.

Wu, Y., Zhang, S., Hao, J., Liu, H., Wu, X., Hu, J., Walsh, M. P., Wallington, T. J., Zhang, K. M., & Stevanovic, S. (2017). On-road vehicle emissions and their control in China: A review and outlook. *Science of The Total Environment*, *574*, 332–349. https://doi.org/10.1016/J.SCITOTENV.2016.09.040

695 Zhang, K., Chen, G., Zhang, Y., Liu, S., Wang, X., Wang, B., & Hang, J. (2020). Integrated impacts of
696 turbulent mixing and NOX-O3 photochemistry on reactive pollutant dispersion and intake
697 fraction in shallow and deep street canyons. *Science of the Total Environment*, *712*, 135553.

698